Jones, R., Melnyk, O., Macedo, R. and Camley, R. E. (2021) Vertically stacked soliton-like domain walls in nematic liquid crystals. *Advanced Theory and Simulations*, 4(11), 2100252.

(doi: 10.1002/adts.202100252)

This is the Author Accepted Manuscript.

There may be differences between this version and the published version. You are advised to consult the publisher's version if you wish to cite from it.

https://eprints.gla.ac.uk/251095/

Deposited on: 6 August 2021

Enlighten – Research publications by members of the University of Glasgow
http://eprints.gla.ac.uk

Vertically Stacked Soliton-Like Domain Walls in Nematic Liquid Crystals

Reed Jones, Olha Melnyk, Rair Macêdo, and Robert E. Camley*

R. Jones, Dr. O. Melnyk, Prof. R. E. Camley
UCCS BioFrontiers Center and Department of Physics and Energy Science, University of Colorado Colorado Springs, Colorado Springs, 80918 USA
E-mail: rjones12@uccs.edu

Dr. O. Melnyk
Herman B Wells Center for Pediatric Research, Department of Pediatrics, Indiana University School of Medicine, Indianapolis, Indiana, 46202 USA

Dr. R. Macêdo
James Watt School of Engineering, Electronics & Nanoscale Engineering Division, University of Glasgow, Glasgow, G12 8QQ UK

Keywords: domain walls, liquid crystals, oscillatory states, metastable states, energy minimization calculations

In the standard liquid crystal geometry, one generally finds a quasi-parabolic director profile in the vertical direction, where the directors are aligned with an applied field in the center of the cell. In contrast, using a numerical energy minimization approach, we find that there are multiple metastable solutions where the director profile is oscillatory. At low voltages, we find small oscillations, which evolve into standard soliton-like domain walls as the applied voltage is increased. We predict the thickness of the domain wall with a simple analytic model that gives a good comparison to our numerical calculations, in the standard domain wall regime. For dual-frequency nematic liquid crystals, the occurrence of this regime can be tuned by a change of the biasing frequency. Moreover, we investigate how domain walls can affect the optical properties of liquid crystal-based devices. For instance, we find that the transmittance curve shifts to higher voltages as domain walls are introduced. This shift can be used to create an efficient tunable filter.

1. Introduction

In a common, planar geometry employing nematic liquid crystals (LC), the LC molecules are often aligned parallel to the surfaces of the LC cell in the absence of a biasing voltage. When a voltage is applied, the LC molecules (as represented by directors) reorient themselves to become aligned with the applied field, similar to an electric dipole in an applied electric field. The reorientation begins in the bulk of the LC cell and extends to the surfaces as the applied field increases. The reorientation at the surfaces is smaller because there is a competition between the anchoring and the elastic energy with the electrostatic energy associated with the applied field.[1–3] **Figure 1**(a) illustrates a typical LC director orientation profile. This transition occurs because LCs are birefringent materials as they have different permittivities and refractive indices in the parallel (extraordinary) and perpendicular (ordinary) directions with respect to the LC director.[4] This tunable difference is used in optical display technology and other applications, including optical filters and tunable microwave devices.[5–9] Dual-frequency nematic LCs share the same properties as ordinary nematic LCs, but they are also tunable with the frequency of the biasing voltage. This can improve the transition speed of LC devices and permit the additional tuning of the dielectric anisotropy to create a tunable filter.[10–12]

While early work concentrated on LC display applications, more recently, topological defects in LCs have become an active area of research. For example, the direction and speed of swimming bacteria can be dynamically controlled using tunable topological defects (i.e. saddle points, sinks, centers, comet orbits and vortices) in various LCs.[13–15] Structured LC elastomers can be designed to behave like piezoelectrics.[16] In a lyotropic colloidal cholesteric LC, nanoparticles can be designed to self-assemble into specific patterns, at the disclinations.[17] Within the last decade, extensive reviews of topological defects in LCs have been published.[18,19] New publications continue to cover a wide range of topological defects. These include active motion of topological defects in LC media,[20] decomposition of center and saddle

point disclinations,[21,22] ionically charged comet orbit and saddle point disclinations in nematic LCs,[23] skyrmions,[24] motile solitons[25] and vortex lattices.[26]

One example of topological defects, in nematic LCs, is the occurrence of horizontal domains. This was first observed in 1961 by Zvereva and Kapustin then studied in depth by Williams in 1963.[2,27] In 1968, Helfrich explained the Kapustin-Williams domains as alignment inversion walls or solitons with magnetic fields.[28,29] Thereafter, solitons have been of great interest in LCs.[30]

Nearly all of the topological defects and domains studied in LC systems have been horizontal, in the sense that the variation in the directions of the LC directors took place parallel to the surface of the LC cell. Very recently, it has been shown, both theoretically and experimentally that one could obtain domains in the vertical direction. All of these works, however, required the application of a strong magnetic field.[31–35]

In this paper, we explore these vertically stacked domains and their consequences in a standard nematic LC geometry, as seen in Figure 1(b). Our theoretical results are obtained from an energy minimization approach; however, one obtains the same results by solving the usual differential equation for the director profile. In contrast to earlier work, we find that these domains are stable even in the absence of a magnetic field. Furthermore, we show that the number of standard domains that can exist as metastable states depends critically on the applied voltage as well as the thickness of the cell. We also quantify the width and energy cost of the domain wall in this configuration and present a physical argument for why oscillations, rather than standard domain walls, occur for small, applied fields. Finally, we show that switching between the usual ground state and a metastable state, can create an optical filter.

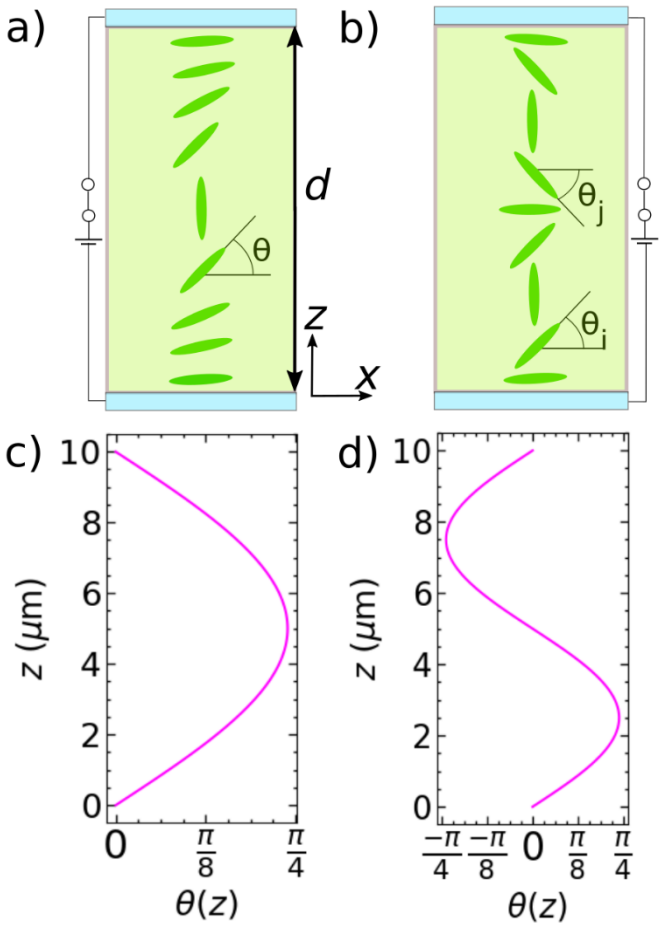

Figure 1. (color online). Schematics of the nematic LC director profile for the (a) ground state and (b) metastable state with one domain wall. The nematic LC is sandwiched between two substrates, each of which contains glass, indium tin oxide for the conductivity and polyimide for the initial LC orientation. (c) Shows the plot of the director profile for the schematic drawing in (a). (d) Shows the plot of the director profile for the schematic drawing in (b).

2. Theoretical Methods – Energy Minimization

The total free energy for a nematic LC in the planar cell arrangement can be found from the sum of the bulk and surface energies, given by

$$F = \int_0^d dz\, U(\theta, \theta') + \frac{1}{2} W \sin^2(\theta - \theta_0) + \frac{1}{2} W \sin^2(\theta \pm \theta_d) \qquad (1)$$

where our surface terms are of the Rapini Papoular form,[4,36] θ_0 and θ_d are the pre-tilt angles at the $z = 0$ and $z = d$ surfaces, respectively and the $\pm$ in the $z = d$ surface term depends on the

initial molecule orientations, created by the surface treatments.[4] Here, the bulk energy density, *U(θ,θ′)*, is a sum of the Oseen-Frank (elastic)[37,38] and the electrostatic[39] energy densities, and given by:

$$U(\theta,\theta') = \frac{1}{2}(K_{11}\cos^2\theta + K_{33}\sin^2\theta)\left(\frac{d\theta}{dz}\right)^2 - \frac{1}{2}\varepsilon_0 E^2(\varepsilon_\perp - \Delta\varepsilon\sin^2\theta). \quad (2)$$

In Equation (1) and (2), *θ(z)* is the angle of the director with respect to the substrate (as shown in Figure 1(a) and (b)), $\theta' = d\theta/dz$, *W* is the anchoring energy, K_{11} and K_{33} are the splay and bend elastic constants, respectively, *E* is the electric field from the applied voltage, ε_0 is the permittivity of free space, and the dielectric anisotropy is $\Delta\varepsilon = \varepsilon_\parallel - \varepsilon_\perp$ where $\varepsilon_\parallel$ and $\varepsilon_\perp$ are the permittivities parallel and perpendicular to the electrodes, respectively. The dielectric anisotropy is quasistatic, and its measurement is used in the free energy minimization. The birefringence or optical anisotropy (Δn) depends on the frequency of the electromagnetic wave passing through the LC cell. This difference means that we cannot change between the two using: $\varepsilon_r = n^2$ as is the typical case in electromagnetism for nonmagnetic materials.[40]

We have numerically minimized the free energy F to solve for the director profile, *θ(z)*. We discretize the z direction with an equally spaced lattice, i.e. $z_n = an$, where *n* ranges from 1 to *N*, and *N* is the number of lattice points and $a = d/N$. We calculate the derivative θ' using a combination of forward and backward difference derivatives. Note that we have neglected any electrostatic charging in the polyimide layers as is often the case in the literature.[41]

The energy minimization is accomplished by guessing an initial configuration, *θ(z)*, then going to a particular position, *z*, varying the angle at that position by a small random amount, and accepting that variation if the energy of the system is lowered. To find an oscillatory metastable state, numerically, we use an initial configuration to be a profile with a domain wall.

3. Results

Unless otherwise specified, we will be using the parameters appropriate for the commercially available MLC-2048 (Merck Ltd), a dual-frequency nematic LC, which is well studied in the literature.[42–44] The Frank elastic constants are K_{11} = 12.4 pN and K_{33} = 24.7 pN;[45] we take a pre-tilt angle of 0.04 rad and an anchoring strength of $W = 2 \times 10^{-4}$ J m^{-2}.[12] We found the wavelength-dependent refractive indices using the Cauchy coefficients: $A_e = 1.6950$, $B_e = -0.0015$ μm^2, $C_e = 0.0035$ μm^4, $A_o = 1.5200$, $B_o = -0.0212$ μm^2 and $C_o = 0.0044$ μm^4 , with a biasing voltage frequency of 1 kHz.[46] We have neglected temperature effects and used SI units throughout.

3.1. Energy Minimization

Using the energy minimization method, the initial guess determines, in part, the stable or metastable state to which the system converges. For example, any of the configurations shown in the initial states plot in **Figure 2**(a) give the same resulting final state shown in the final configuration plot in Figure 2(a), after the energy minimization process is complete. The plot of the ground state is for a 10-micron LC cell at a voltage of 25 V.

When the initial configuration is oscillatory, as shown in the initial states plot in Figure 2(b), we find the system converges to a metastable oscillatory final state with a soliton-like domain wall as shown in the final configuration plot in Figure 2(b), after the energy minimization process is complete. The plot of the oscillatory state is for a 10-micron LC cell at a voltage of 25 V. We note that an initial state oscillation involving all positive angles is not stable and will converge to the typical ground state configuration.

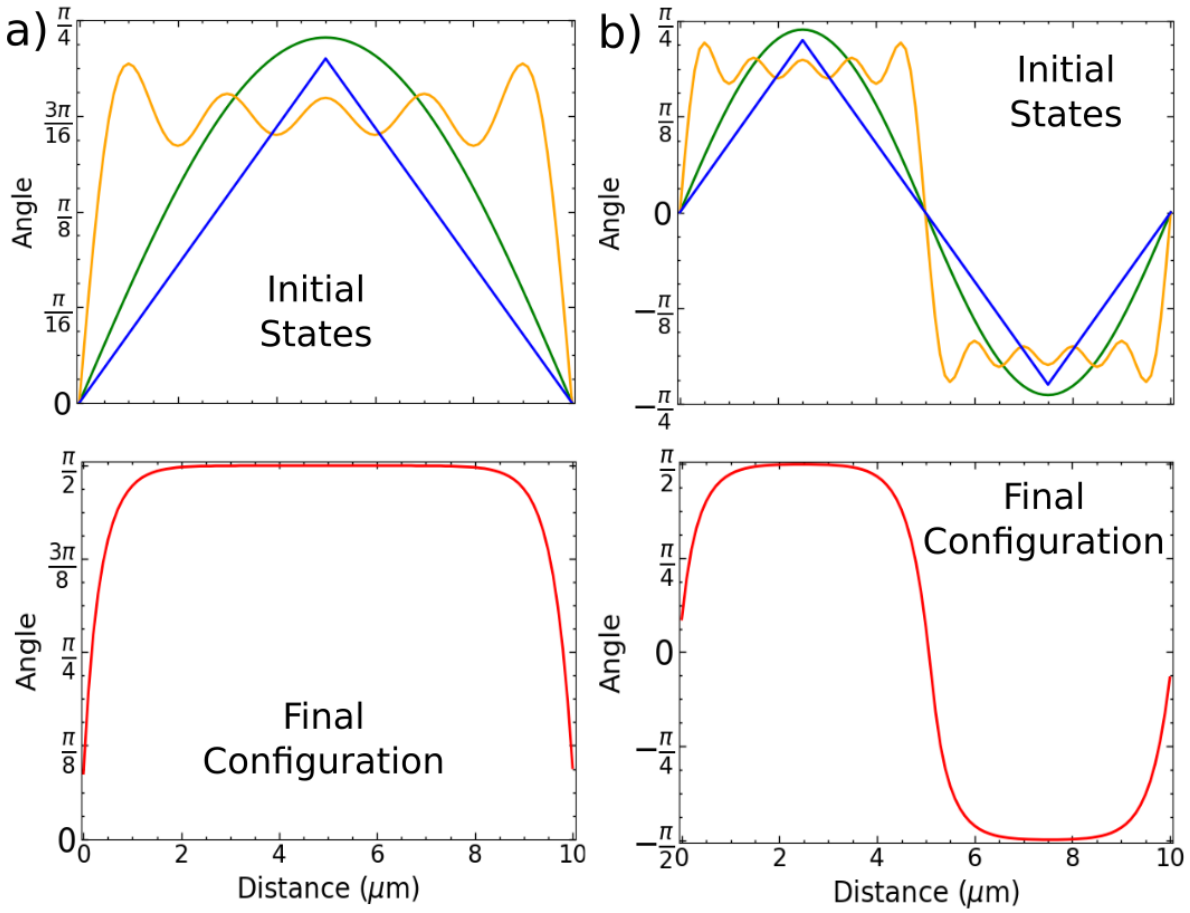

Figure 2. (color online) Director angle as a function of vertical position in the LC cell for (a) initial states that give the final configuration, of the ground state, at 25 V and (b) initial states that give the final configuration, of a one domain wall oscillatory state, at 25 V.

We deduce that an oscillatory initial profile is required to numerically find an oscillatory metastable state using energy minimization. All three initial configurations in Figure 2(b) collapse into the same oscillatory metastable state. These oscillatory solutions can also be found through the differential equation for the director profile.

3.2. Domain Wall Width and Energy Cost

In the metastable state, as seen in Figure 2(b), the LC directors form a domain wall near the center of the cell. In **Figure 3**, we show how the domain walls and metastable state configurations depend on the voltage across the cell for two sample metastable states.

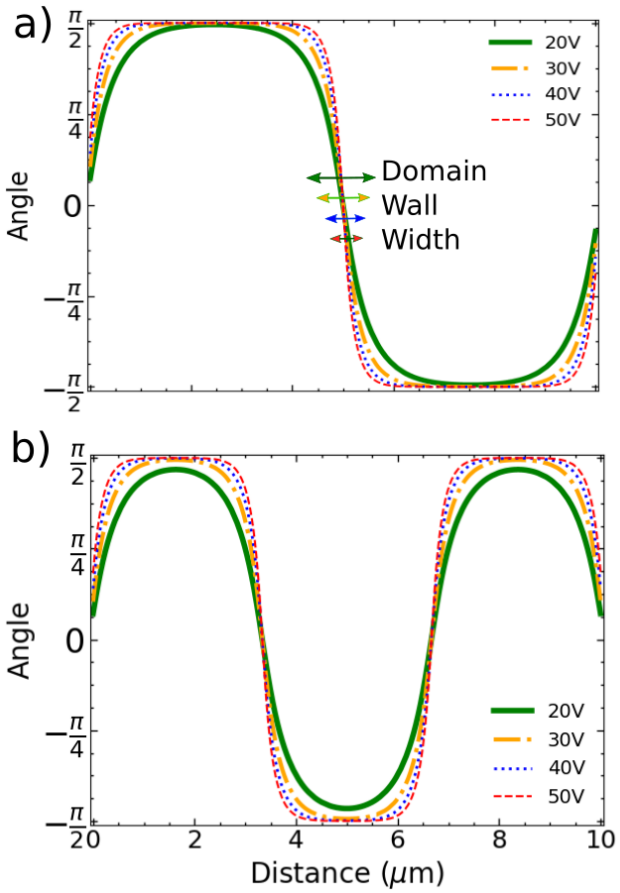

Figure 3. (color online) Director angle as a function of vertical position in the LC cell, for metastable states at different voltages. This illustrates that domain walls become smaller as the voltage increases for (a) one and (b) two domain-wall configurations.

It is clear that the domain walls become narrower as the voltage is increased. We want to create a simple analytic model to predict the width of the domain walls. This will allow us to compare our numerical results with an analytic prediction. To do this, we assume a variational solution for the director angle in the domain wall, of width δ, and a linear dependence of the director angle on position. For simplicity in the calculation, we define a new coordinate axis z', parallel to z but shifted so that, $z' = 0$ is the start of the domain wall.

$$\theta(z') = \frac{\pi}{2} - \frac{\pi z'}{\delta} \tag{3}$$

δ is viewed as a variational parameter. We have subtracted $\pi z'/\delta$ from $\pi/2$ so that at a position of $z' = 0$ and $z' = \delta$ (the start and end of the wall, respectively) we will have the proper angles

of $\pm\pi/2$. For simplicity, we consider the difference in the energy between the metastable state and the ground state only for the region where the domain wall exists in the metastable state. For the ground state, the director angle, in and around the position of the domain wall, is always $\pi/2$. This approximation is reasonably good for moderate voltages (see **Figure 4**(b) and **5**(a)). We subtract the free energy of the ground state from the free energy of the oscillatory state, in the region of the domain wall, to find the cost in energy to build the domain wall, F_{DW}. We obtain

$$F_{DW} = \int_0^{\delta} \left[\frac{1}{2} (K_{11} \cos^2\theta + K_{33} \sin^2\theta) \left(\frac{\partial\theta}{\partial z'} \right)^2 - \frac{1}{2} \varepsilon_0 \Delta\varepsilon \left(\frac{V}{d} \right)^2 (\sin^2\theta - 1) \right] dz'. \quad (4)$$

In deriving this, we have used the assumption of the constant angle of $\pi/2$ for the ground state makes its elastic term disappear due to the spatial derivative. Further, this also makes the $\sin^2$ term go to 1 in its electrostatic energy. Also, the angle independent terms in the electrostatic energy subtract away in obtaining Equation (4). After integrating, we take the partial derivative of the energy of the wall with respect to δ. We set this equal to zero and solve for δ to obtain the thickness of the domain wall. We find the following analytic form

$$\delta = \frac{\pi d}{V} \sqrt{\frac{K_{11} + K_{33}}{\varepsilon_0 \Delta\varepsilon}}. \quad (5)$$

We see that the thickness of the domain wall is inversely proportional to the applied electric field. If we use the value of δ found above, in Equation (5), we can integrate Equation (4) to find the energy cost to build a domain wall. One obtains

$$E = \frac{\pi}{2} \frac{V}{d} \sqrt{\varepsilon_0 \Delta\varepsilon (K_{11} + K_{33})}. \quad (6)$$

We can extend this calculation to a LC with *n* domain walls, by assuming that all domain walls have the same width. This is a good assumption if the walls are in the bulk of the LC cell. Therefore, we multiply the width of one wall by *n* to learn the total thickness of all of the domain walls in the LC cell. If there are a lot of walls, we would expect the ones closer to the surface to have a different width than the ones in the center.

Obviously, this calculation must break down at some point. For states with multiple domain walls, one certainly cannot have the total thickness of the domain walls be larger than the thickness of the LC cell. This suggests that there is a thickness at which the standard domain walls, with θ varying from $+\pi/2$ to $-\pi/2$, can no longer exist. Of course, this critical thickness is likely to occur well below the point where the total domain wall width is equal to the thickness of the LC cell, as will be confirmed below. Because the thickness of the domain walls depends on the electric field, this also suggests the presence of a critical voltage, at a fixed thickness. We explore these ideas below.

In Figure 4(a), we plot the director profile for the case of four domain walls for different values of voltage. At high voltages one obtains the standard domain wall situation, where θ varies from $+\pi/2$ to $-\pi/2$ in a short distance. As the voltage is reduced, however, the situation changes and instead of the rapid soliton-like behavior found at high voltages, one has a simple oscillatory behavior. This occurs because, at low voltages, the electrostatic energy is small compared to the elastic energy, and it is not favorable to have rapid changes in angle as a function of position.

We explored changing the Frank elastic coefficients to determine if there was a limit where elastic forces would prevent an oscillatory metastable state. For realistic Frank elastic coefficients, we were always able to find an oscillatory metastable state. Using an oscillatory

configuration as the initial state, we also did not find a limit as to how many domain walls the director profile can have.

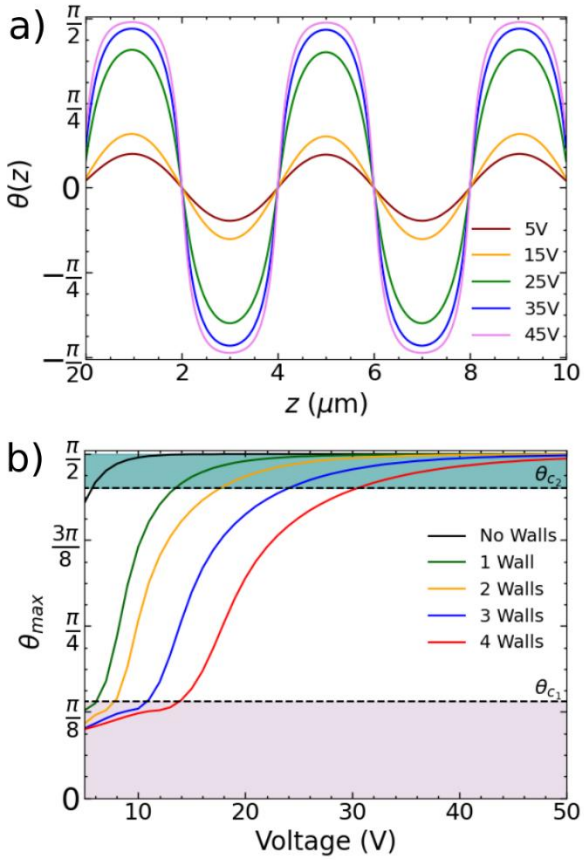

Figure 4. (color online) (a) LC director profile as a function of vertical position in the cell for a 10 μm MLC-2048 LC cell for different applied voltages. There are sinusoidal oscillations at small voltages and standard domain walls at large voltages. (b) The maximum LC director angle as a function of the applied field for a 10 μm MLC-2048 LC cell. We define a critical angle of $\theta_{c_1} = 0.28\frac{\pi}{2} = 25.2°$, because θ_{max} increases substantially as voltage increases, and the domain wall width decreases (see Figure 5(a)). We define a second critical angle of $\theta_{c_2} = 0.9\frac{\pi}{2} = 81°$ to be where standard domains form and the numerical results approach those of the analytic model for standard domains (see Figure 5(a)). Both critical angles shift to higher voltages as the number of domain walls increase and the dielectric anisotropy decreases (see Figure 5(b)).

To quantify the behavior of the domain walls, we plot the maximum angle seen in the configuration, θ_{max}, as a function of voltage for a 10-micron thick cell and for states with different numbers of domain walls in Figure 4(b). It is helpful to define two critical angles. The first one, θ_{c_1}, occurs when the maximum angle starts to rapidly increase near $\theta_{c_1} = 0.28\frac{\pi}{2} = 25.2°$. A second critical angle, θ_{c_2}, is found as the voltage increases and θ_{max}

approaches $\pi/2$. We define the second critical angle, $\theta_{c_2} = 0.9\frac{\pi}{2} = 81°$. Each of these critical angles can be connected to a critical voltage as we will see in Figure 5(a).

The critical voltages have an impact on the domain wall thickness. We measure the domain wall width by finding the maximum angle, and then noting the nearby positions where the θ is 90% of θ_{max} and taking the distance between these two positions. Figure 5(a) shows the domain wall width, with the solid lines representing the results of the analytical formulas, and the symbols showing the behavior calculated from the full numerical calculation. This calculation is done for four different numbers of domain walls for a 10 μm LC cell. At high voltages (above θ_{c_2}, see Figure 4(b)), the two models give nearly equivalent behaviors. At θ_{c_2}, the numerical result crosses over the analytic calculation. As the voltage is reduced, the energy minimization results deviate from the analytic result. As discussed earlier, this is because the $\theta_{max} = \pm\frac{\pi}{2}$ approximations, in the analytic model, are no longer reasonable and we get oscillations instead of soliton-like domain walls in the LC director profiles. At low voltages (below θ_{c_1}, see Figure 4(b)), the domain wall thickness flattens out and even slightly shrinks. At θ_{c_1}, the numerical result reaches its maximum thickness.

For the dual-frequency nematic LC, we can explore how the domain behavior depends on the frequency of the biasing voltage, which effectively adjusts the dielectric anisotropy. From Equation (5), one can see that it is possible to alter the thickness of the domain walls by changing the dielectric anisotropy. A smaller dielectric anisotropy reduces the electrostatic energy. This means that a larger voltage is required to win the competition with the elastic energy. Thus, the width of the domain wall increases as the dielectric anisotropy decreases as seen in Figure 5(b). The symbols do not line up exactly with the analytic model, however, their separation at a given, higher voltage is consistent with the model. Again, the deviation between the two sets of results occurs near a critical voltage as seen in Figure 4(b) and 5(a).

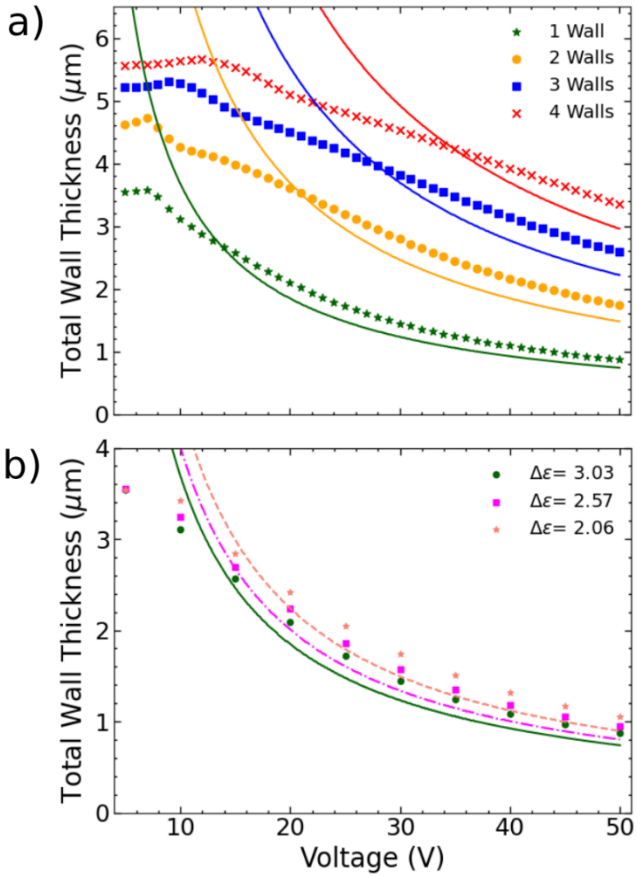

Figure 5. (color online) (a) Total domain wall/oscillation thickness as a function of the applied voltage for a 10 μm, MLC-2048 LC cell for four different number of domain walls. The numerical model results (symbols) are close to those of the analytic model (lines) for higher voltages. (b) Total domain wall/oscillation thickness as a function of the applied voltage for a 10 μm, MLC-2048 LC cell for three different dielectric anisotropies in a one domain-wall configuration. As the dielectric anisotropy decreases (biasing voltage frequency increases), the thickness of the wall increases. The lines are the values obtained from the analytic model and the symbols are from the numerical energy minimization model.

3.3. Energy Cost of a Domain Wall

It is of interest to identify the energy of the states with different numbers of domain walls. This is presented in **Figure 6**. As expected, the ground state has the lowest areal energy density, and increasing the number of domains slightly raises the energy density. We can understand the spacing between the different cases through Equation (6) which shows that the cost of a domain wall is proportional to the voltage.

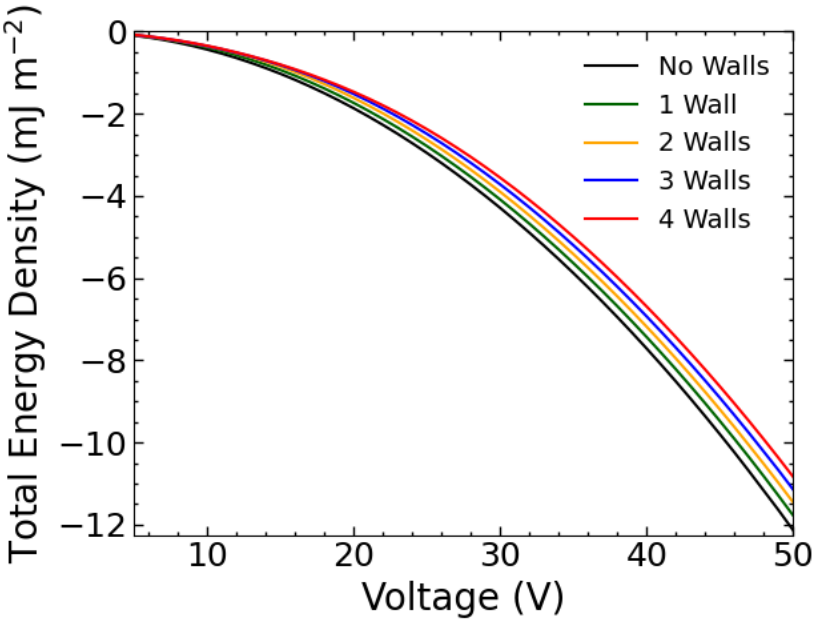

Figure 6. (color online) Total energy density as a function of the biasing voltage for the ground state and four different numbers of domain walls. All curves are for a 10 μm MLC-2048 LC cell.

3.4. Transmittance

Electro-optical measurements are the most ubiquitous way to study LC director profiles. Here we study how the change in director profile, from the ground state to a state with domain walls, influences the transmittance through the LC cell. The theoretical methods for this is well established, so we do not present any details here.[12,47] We will use the geometry presented in Figure 1(a) and 1(b) with the LC cell sandwiched between a +45° polarizer on top and -45° polarizer on bottom, forming a LC retarder. We place the LC retarder between a laser and a detector to create a straight optical pass configuration.[48]

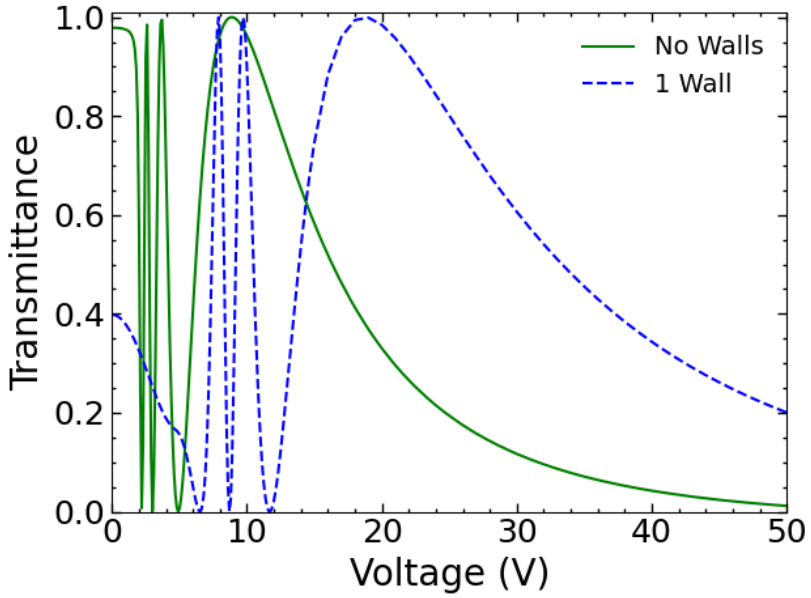

Figure 7. (color online) Transmittance as a function of voltage for a single LC cell between crossed polarizers with an incident light wavelength of 632 nm. Both curves are for a 10 μm MLC-2048 LC cell. The solid green line is the transmittance curve for a LC cell in the ground state, and the blue dashed curve depicts the transmittance for the case where there is one domain wall.

In **Figure 7**, we plot the transmittance as a function of voltage for the ground state and for the state with one domain wall. For the ground state, there is a final broad peak around 10 V and the transmittance of this peak's tail goes to zero as the voltage increases. In contrast, in the oscillatory metastable state, the broad peak of the transmittance curve is shifted to higher voltages. At low voltages, in the metastable state, the director profile is comprised of small oscillations. There is a transition between where the one wall transmittance curve is irregular and where it looks shifted from the no walls curve around 5 V. This transition is near the critical voltage, associated with the critical angle, θ_{c_1} (see Figure 4(b) and 5(a)). Additional domain walls shift the transmittance curve to higher voltages.

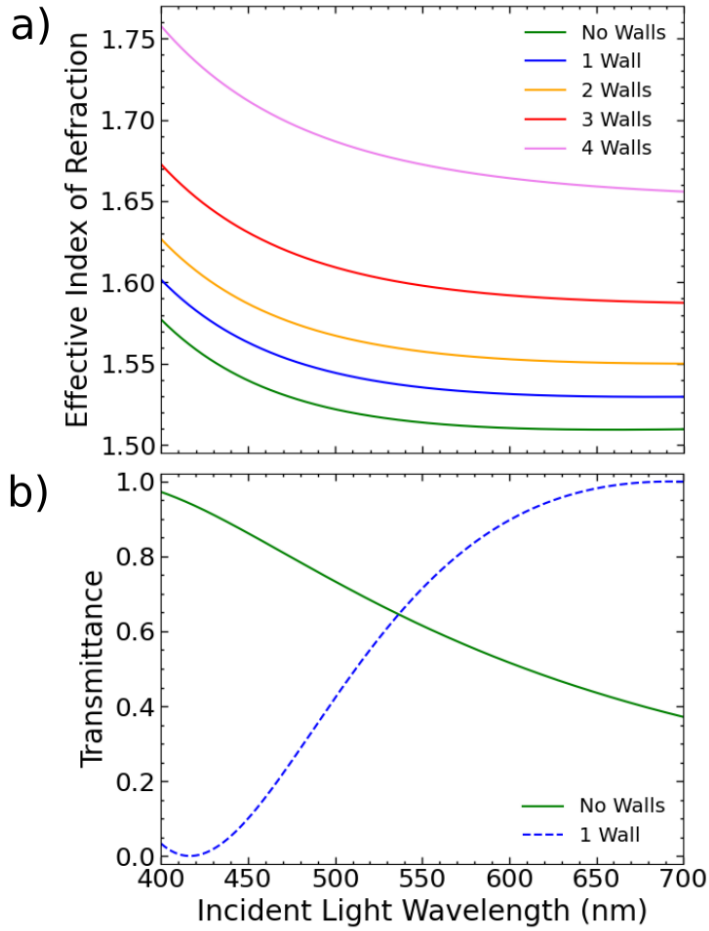

Figure 8. (color online) (a) Effective index of refraction as a function of incident light wavelength for a single LC cell between crossed polarizers with an applied field of 17 V. All curves are for a 10 μm MLC-2048 LC cell. The green line is the effective refractive index curve for a LC cell in the ground state. The blue, orange, red and violet lines depict the effective index of refraction for the case where there is one, two, three and four domain walls, respectively. (b) Transmittance as a function of incident light wavelength for a single LC retarder with an applied field of 17 V. Both curves are for a 10 μm MLC-2048 LC cell. The solid green line is the transmittance curve for a LC cell in the ground state, and the blue dashed curve depicts transmittance for the case where there is one domain wall.

The effective index of refraction, in the LC cell, depends on the number of domain walls. As the number of domain walls is increased, the effective refractive index increases, as seen in **Figure 8**(a). The spacing between the curves becomes larger as the number of walls increase.

Because the index of refraction depends strongly on the number of domain walls, this could, in principle, be used to create a tunable filter. In Figure 8(b), we plot transmittance as a function of the wavelength of the incident light for the ground state and one domain wall state.

We see that at 420 nm the transmittance is nearly 1 for the ground state, and nearly zero for the one domain wall state, indicating a potential to create an efficient filter for these wavelengths.

4. Conclusion and Discussions

In this paper, we have investigated the possibility of domain walls along the vertical axis in a typical nematic LC cell. We find that metastable states do exist at any voltage. We used a simple variational model to calculate the thickness of the domain wall and compared the results with a numerical energy minimization approach. We found that the analytic and numeric approaches give comparable values, for the domain wall thickness, above a critical voltage. Indeed, for larger voltages, we find that the domain wall is similar to a soliton. Below that critical voltage, the domain wall thickness continues to increase, but no longer follows the analytic model. Furthermore, at low voltages, we find that instead of a large change in the director angle (from $+\pi/2$ to $-\pi/2$) the maximum director angle becomes smaller, and the director profile is oscillatory instead of having distinct domain walls.

We find that the transmittance depends strongly on the director profile, with significant differences occurring with and without domain walls. This suggests a novel approach to create a filter by switching between the ground state and oscillatory metastable state. This also permits transmittance at higher voltages. This work may be expanded by exploring Bragg reflections in the LC cell, particularly for thicker films with multiple domain walls.

Finally, it would be fruitful to explore the dynamical process that the LC director undergoes as it reorients into the final oscillatory states described in this work. However, this would significantly complicate the present study. Some notable advantages of this dynamical investigation are: clarification as to how the metastable states are reached, the speed of reorientation[35] and insight into the impact of dual-frequency.

Acknowledgements. This work was supported by the UCCS BioFrontiers Center, University of Colorado Colorado Springs.

Conflict of Interest. The authors declare no conflict of interest.

References

1. de Gennes, P.G., and Prost, J. (1993) *The physics of liquid crystals*, Oxford University Press, New York.

2. Blinov, L.M., and Chigrinov, V.G. (1993) *Electro-optic effects in liquid crystal materials*, Springer, New York.

3. Fréedericksz, V., and Zolina, V. (1933) Forces causing the orientation of an anisotropic liquid. *Trans. Faraday Soc.*, **29** (140), 919–930.

4. Yang, D.-K., and Wu, S.-T. (2015) *Fundamentals of liquid crystal devices*, John Wiley & Sons, Ltd.

5. Aharon, O., and Abdulhalim, I. (2009) Tunable optical filter having a large dynamic range. *Opt. Lett.*, **34** (14), 2114–2116.

6. Patel, J.S., Saifi, M.A., Berreman, D.W., Lin, C., Andreadakis, N., and Lee, S.D. (1990) Electrically tunable optical filter for infrared wavelength using liquid crystals in a Fabry-Perot étalon. *Appl. Phys. Lett.*, **57** (17), 1718–1720.

7. Garbovskiy, Y., Zagorodnii, V., Krivosik, P., Lovejoy, J., Camley, R.E., Celinski, Z., Glushchenko, A., Dziaduszek, J., and Dąbrowski, R. (2012) Liquid crystal phase shifters at millimeter wave frequencies. *J. Appl. Phys*, **111** (5), 054504.

8. Camley, R., Celinski, Z., Garbovskiy, Y., and Glushchenko, A. (2018) Liquid crystals for signal processing applications in themicrowave andmillimeter wave frequency ranges. *Liq. Cryst. Rev.*, **6** (1), 17–52.

9. Nobles, J.E., Melnyk, O., Glushchenko, A., Camley, R.E., and Celinski, Z. (2020) Effect of alignment methods on liquid crystal performance in millimeter wave devices. *Eng. Res. Express*, **2** (2), 025002.

10. Melnyk, O., Garbovskiy, Y., and Glushchenko, A. (2020) Order parameter of dual-frequency nematic liquid crystals measured over a wide range of thicknesses. *Liq. Cryst.*, **47** (9), 1338–1344.

11. Wu, S.-T. (1989) Design of a liquid crystal based tunable electrooptic filter. *Appl. Opt.*, **28** (1), 48.

12. Melnyk, O., Jones, R., Macêdo, R., Garbovskiy, Y., Hagen, G., Glushchenko, A. V, Spendier, K., and Camley, R.E. (2021) Fast switching dual-frequency nematic liquid crystal tunable filters. *ACS Photonics*, **8** (4), 1222–1231.

13. Genkin, M.M., Sokolov, A., Lavrentovich, O.D., and Aranson, I.S. (2017) Topological defects in a living nematic ensnare swimming bacteria. *Phys. Rev. X*, **7** (1), 011029.

14. Kawaguchi, K., Kageyama, R., and Sano, M. (2017) Topological defects control collective dynamics in neural progenitor cell cultures. *Nature*, **545** (7654), 327–331.

15. Peng, C., Turiv, T., Guo, Y., Wei, Q.-H., and Lavrentovich, O.D. (2016) Command of active matter by topological defects and patterns. *Science (80-.).*, **354** (6314), 882–885.

16. Guin, T., Settle, M.J., Kowalski, B.A., Auguste, A.D., Beblo, R. V., Reich, G.W., and White, T.J. (2018) Layered liquid crystal elastomer actuators. *Nat. Commun.*, **9** (1), 1–7.

17. Li, Y., Prince, E., Cho, S., Salari, A., Golestani, Y.M., Lavrentovich, O.D., and Kumacheva, E. (2017) Periodic assembly of nanoparticle arrays in disclinations of cholesteric liquid crystals. *Proc. Natl. Acad. Sci. U. S. A.*, **114** (9), 2137–2142.

18. Araki, T., Serra, F., and Tanaka, H. (2013) Defect science and engineering of liquid crystals under geometrical frustration. *Soft Matter*, **9** (34), 8107–8120.

19. Serra, F. (2016) Curvature and defects in nematic liquid crystals. *Liq. Cryst.*, **43**, 1920–1936.

20. Tang, X., and Selinger, J. V (2021) Alignment of a topological defect by an activity gradient. *Phys. Rev. E*, **103** (2), 022703.

21. Wu, J., Liu, M., Zhou, X., and Zhang, Z. (2021) Decomposition of topological defects in liquid crystal wells with homeotropic anchoring. *Liq. Cryst.*, 1–11.

22. Endresen, K.D., Kim, M., Pittman, M., Chen, Y., and Serra, F. (2021) Topological defects of integer charge in cell monolayers. *Soft Matter*, **17** (24), 5878–5887.

23. Everts, J.C., and Ravnik, M. (2021) Ionically charged topological defects in nematic fluids. *Phys. Rev. X*, **11** (1), 011054.

24. Duzgun, A., and Nisoli, C. (2021) Skyrmion spin ice in liquid crystals. *Phys. Rev. Lett.*,

126 (4), 047801.

25. Aya, S., and Araoka, F. (2020) Kinetics of motile solitons in nematic liquid crystals. *Nat. Commun.*, **11**, 3248.

26. Calisto, E., Clerc, M.G., and Zambra, V. (2020) Magnetic field-induced vortex triplet and vortex lattice in a liquid crystal cell. *Phys. Rev. Res.*, **2** (4), 042026.

27. Williams, R. (1963) Domains in liquid crystals. *J. Chem. Phys*, **39** (2), 384–388.

28. Helfrich, W. (1968) Alignment-inversion walls in nematic liquid crystals in the presence of a magnetic field. *Phys. Rev. Lett.*, **21** (22), 1518–1521.

29. Helfrich, W. (1969) Errata: Alignment-inversion walls in nematic liquid crystals in the presence of a magnetic field. *Phys. Rev. Lett.*, **22** (24), 1342.

30. Lam, L., and Prost, J. (eds.) (1992) *Solitons in liquid crystals*, Springer New York, New York, NY.

31. Zakharov, A. V., and Vakulenko, A.A. (2013) Dynamics of the modulated distortions in confined nematic liquid crystals. *J. Chem. Phys.*, **139** (24), 244904-1–6.

32. Vakulenko, A.A., and Zakharov, A. V (2013) Field-induced director dynamics in confined nematic liquid crystals imposed by a strong orthogonal electric field. *Phys. Rev. E*, **88** (2), 022505-1–7.

33. Zakharov, A. V. (2016) Peculiarities in the director reorientation and evolution of NMR spectra under the influence of crossed electric and magnetic fields. *Phys. Solid State*, **58** (12), 2580–2586.

34. Zakharov, A. V., Vakulenko, A.A., and Pasechnik, S. V. (2016) Reorientation dynamics of nematics encapsulated in microscopic volumes in a strong electric field. *Phys. Solid State*, **58** (9), 1916–1923.

35. Zakharov, A. V, Maslennikov, P. V, and Pasechnik, S. V (2021) Electrically driven nematic flow in microfluidic capillary with radial temperature gradient. *Phys. Rev. E*, **103**, 12702.

36. Rapini, A., and Papoular, M. (1969) Distorsion d'une lamelle nématique sous champ

magnétique conditions d'ancrage aux parois [Distortion of a nematic lamella under magnetic field conditions anchoring to the walls]. *J. Phys. Colloq.*, **30** ((C4)), 54–56.

37. Frank, F.C. (1958) On the theory of liquid crystals. *Discuss. Faraday Soc.*, **25**, 19–28.

38. Oseen, C.W. (1933) The theory of liquid crystals. *Trans. Faraday Soc.*, **29**, 883–899.

39. Scolari, L., Bjarklev, A.O., Eskildsen, L., and Alkeskjold, T.T. (2009) Liquid crystals in photonic crystal fibers: fabrication, characterization and devices.

40. Griffiths, D.J. (2013) *Introduction to electrodynamics*, Pearson Education.

41. Chen, P.A., and Yang, K.H. (2018) Ionic effects on electro-optics and residual direct current voltages of twisted nematic liquid crystal cells. *Liq. Cryst.*, **45** (7), 1032–1039.

42. Melnyk, O., Garbovskiy, Y., Bueno-Baques, D., and Glushchenko, A. (2019) Electro-optical switching of dual-frequency nematic liquid crystals: Regimes of thin and thick cells. *Crystals*, **9** (6), 1–8.

43. Golovin, A.B., Shiyanovskii, S. V, and Lavrentovich, O.D. (2003) Fast switching dual-frequency liquid crystal optical retarder, driven by an amplitude and frequency modulated voltage. *Appl. Phys. Lett.*, **83**.

44. Wen, C.-H., and Wu, S.-T. (2005) Dielectric heating effects of diual-frequency liquid crystals. *Appl. Phys. Lett.*, **86**, 231104.

45. Wang, C.-T., Tam, A., Tseng, M.-C., Lee, C.-Y., Lin, T.-H., and Kwok, H.-S. (2019) Bistable switching of polarization-grating diffractions enabled by a front bistable twisted nematic film. *Opt. Lett.*, **44** (2), 187.

46. Xiong, J., Chen, R., and Wu, S.-T. (2019) Device simulation of liquid crystal polarization gratings. *Opt. Express*, **27** (13), 18102.

47. Scharf, T. (2007) *Polarized light in liquid crystals and polymers*, Wiley-Interscience, Hoboken, New Jersey.

48. Kumar, S. (ed.) (2001) *Liquid crystals: experimental study of physical properties and phase transitions*, Cambridge University Press, Cambridge.

In the standard liquid crystal geometry, one generally finds that the liquid crystal molecules align with the applied field. In contrast, the authors found that there are multiple metastable solutions where the liquid crystal molecules orientation is oscillatory and can converge into periodic soliton-like solutions. The authors predict the thickness of the soliton-like domain wall with a simple analytic model.

Reed Jones*, Olha Melnyk, Rair Macêdo, and Robert E. Camley

Vertically Stacked Soliton-Like Domain Walls in Nematic Liquid Crystals